AIP Advances

Annealing-induced change in quantum dot chain formation mechanism

Tyler D. Park, John S. Colton, Jeffrey K. Farrer, Haeyeon Yang, and Dong Jun Kim

Citation: AIP Advances **4**, 127142 (2014); doi: 10.1063/1.4905053
View online: http://dx.doi.org/10.1063/1.4905053
View Table of Contents: http://scitation.aip.org/content/aip/journal/adva/4/12?ver=pdfcov
Published by the AIP Publishing

Annealing-induced change in quantum dot chain formation mechanism

Tyler D. Park,[1] John S. Colton,[1,a] Jeffrey K. Farrer,[1] Haeyeon Yang,[2] and Dong Jun Kim[3]
[1]*Department of Physics and Astronomy, Brigham Young University, Provo UT 84602, USA*
[2]*Department of Nanoscience and Nanoengineering, South Dakota School of Mines and Technology, Rapid City, SD 57701, USA*
[3]*IPG Photonics Corporation, Oxford, MA 01540, USA*

(Received 26 September 2014; accepted 15 December 2014; published online 22 December 2014)

Self-assembled InGaAs quantum dot chains were grown using a modified Stranski-Krastanov method in which the InGaAs layer is deposited under a low growth temperature and high arsenic overpressure, which suppresses the formation of dots until a later annealing process. The dots are capped with a 100 nm GaAs layer. Three samples, having three different annealing temperatures of 460°C, 480°C, and 500°C, were studied by transmission electron microscopy. Results indicate two distinct types of dot formation processes: dots in the 460°C and 480°C samples form from platelet precursors in a one-to-one ratio whereas the dots in the sample annealed at 500°C form through the strain-driven self-assembly process, and then grow larger via an additional Ostwald ripening process whereby dots grow into larger dots at the expense of smaller seed islands. There are consequently significant morphological differences between the two types of dots, which explain many of the previously-reported differences in optical properties. Moreover, we also report evidence of indium segregation within the dots, with little or no indium intermixing between the dots and the surrounding GaAs barrier. [http://dx.doi.org/10.1063/1.4905053]

In recent decades, quantum dots (QDs) have received large interest in the scientific community.[1] Due to their discrete and tunable wavelength emission as well as their localized electronic states, quantum dots have potential applications as lasers,[2] detectors,[3] optoelectronic devices,[4] and quantum computing.[5] Quantum dot size and morphology play a large role in the optical and electronic properties,[6] therefore investigations into growth techniques which allow for greater control of the geometry and chemical composition are warranted. The most common technique for the self-assembly of epitaxial QDs is the Stranski-Krastanov (SK) method,[7] where (for example) an InGaAs layer is grown on a GaAs substrate at temperatures of around 500°C. The strain mismatch causes the InGaAs layer to spontaneously form into dots once the layer reaches a critical thickness.

A new approach toward self-assembly has been used by several groups to achieve a greater control of the resulting growth.[8–11] In this modified SK technique, an InGaAs layer is grown at a cooler temperature than in the traditional technique, and under a high arsenic overpressure—both of which suppress the formation of dots by suppressing the detachment of atoms from the strained layer due to the low thermal energy. This allows the InGaAs layer to grow thicker than the traditional critical thickness for spontaneous dot formation. Instead, the dots form at later annealing stages when the temperature is sufficiently increased. These modifications introduce new control variables into the growth process, such as InGaAs layer thickness and annealing temperature. By adjusting these and other growth parameters, Kim *et al*. were able to affect the shape and morphology of

[a]E-mail: john_colton@byu.edu

the dots; for example, the dots could be formed into self-assembled chains.[9] In addition to allowing for interesting morphologies, the low temperature growth is believed to suppress deleterious effects of indium segregation (indium clumping at the top of dots), evaporation, and intermixing (indium seeping into the substrate from the wetting layer),[12,13] which cause inhomogeneity in the indium concentration. Chaining of dots has also been obtained using other techniques such as e-beam lithography[14] and cleaved edge overgrowth,[15] superlattice growth,[16,17] and exploiting strain fluctuations in dislocation-patterned templates[18]—but these typically involve an underlying pattern whereas the low temperature modified SK growth technique allows chain formation through self-assembly of dots into chains from a single InGaAs layer.

The three samples we have studied in this work are all QD chain samples grown via the modified, low temperature growth SK technique. Each of the three samples contains a single stack of QD chains grown by depositing approximately 10 monolayers of $In_{0.40}Ga_{0.60}As$ by molecular beam epitaxy (MBE), then annealing at temperatures of 460°C, 480°C, and 500°C. For simplicity, we will call the samples annealed at temperatures 460°C, 480°C, and 500°C, samples A, B, and C respectively. The samples were annealed for 120 seconds; immediately after, 10 nm of GaAs were deposited on top of the InGaAs, forming a preliminary capping layer. An additional nominal 90 nm of GaAs was thereafter deposited at a higher temperature of 580°C, resulting in a total capping layer of about 100 nm (the capping layer for sample B was somewhat less than this). A schematic of the final product is shown in Figure 1. Additional details on the growth technique and optical properties can be found in reference;[19] to summarize, analysis of the RHEED patterns suggest that the QD-chains of samples A and B actually form after the annealing, as the sample temperature approaches or reaches the higher temperature of cap layer growth (580°C), whereas the QD-chains of sample C likely form just prior to reaching its annealing temperature (i.e. just below 500°C). Samples A and B exhibited outstanding optical properties such as exceptionally narrow low temperature photoluminescence (PL) linewidths (<20 meV) and substantial PL visible at room temperature, and in many respects resembled each other and differed from sample C (which had similar optical properties to traditional SK dots). This caused us to propose that the differences in optical properties may arise from structural differences induced by differences in the dot formation processes. (The dot formations processes were clearly different for A and B as compared to C, because the chevrons in the RHEED pattern which typically indicate the formation of dots were absent for samples A and B during the whole growth process.) In this work we show that substantial structural differences do indeed exist between the two types of dots. Samples A and B have a larger number of smaller dots, whereas sample C exhibits a smaller number of larger (but shorter) dots. This may indicate that to improve optical properties of quantum dots, one should do a cooler anneal followed by a fast raise in temperature. Moreover, we also report evidence that there is indium segregation within the dots, but little or no indium intermixing with the GaAs barrier outside the dots. This indicates that suppressing intermixing is far more important towards obtaining good optical properties than suppressing segregation.

We analyzed the structural differences between dots using transmission electron microscopy (TEM). Our TEM images were mainly taken with a Tecnai TF-30 TEM with a 300 keV beam, in both plan-view and cross-section view. In order to image the dots, we used the diffraction contrast

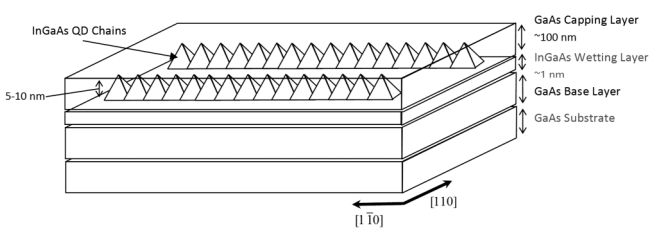

FIG. 1. Schematic diagram of a QD chain sample. The samples are reported to be pyramidal in shape[9] and often overlap partially from dot to dot.

method with a (220) two-beam condition. This creates visible strain contrast due to lattice distortions on the (220) planes which are caused by the self-assembled QDs. Techniques for imaging the dots in our samples are similar to those explained in Reference 20.

In order for the 300 keV beam to pass through GaAs samples, the samples must be less than 100 nm thick; we therefore had to develop methods for preparing different "cuts" (very small pieces) of the samples which included the dot-containing regions. To obtain cross-section cuts, we performed a lift-out via a FEI Helios Nanolab 600 FIB/SEM scanning electron microscope (SEM) with a Ga^+ focused ion beam (FIB) mill.[21] This is done by milling out a pit on either side of a 1 μm × 10 μm rectangle, to a depth of ~5 μm (see Figure 2a). The 1 × 10 × 5 μm cut is then attached to an OmniProbe needle, separated from the substrate, lifted out from the pit, and mounted on a copper TEM grid where it is thinned further with the FIB to final dimensions of ~0.1 × 10 × 5 μm. Chemical analysis was performed on the cross-section cuts on a Tecnai TF20 analytical transmission electron microscope equipped for energy dispersive X-ray spectroscopy (XEDS or EDS). The beam size for the EDS analysis was typically smaller than 1 nm × 1 nm. Line scans were performed via a sequence of points taken across the InGaAs region (wetting layer and dots), having dwell times of 10-20 s. Images from the cross-section cuts were used to characterize both the height of the strain field produced by the dots and the distribution of indium across the dot layer.

Plan-view cuts were obtained using a slightly different method. For sample C, the cut was prepared in a lift-out method similar to the cross-section cuts; see Figure 2b. In this case, a pit is milled out from the edge just below the intended cut, then the cut is bonded to the OmniProbe needle and lifted out. However, this proved challenging to reproduce. Therefore for samples A and B, we used a hybrid method of hand polishing and FIB thinning.[22] In this method, we attach part of the sample to a tripod polisher and thin the sample down close to 1 μm, at approximately a 1° angle; see Figure 3. The sample is then mounted to a copper half-washer and an area is thinned to the required 100 nm with the FIB, resulting in a usable portion with final dimensions of approximately 0.1 × 20 × 5 μm. TEM images from the plan-view cuts were used to characterize dot sizes, dot spacings within chains, the spacings between chains, and overall dot density.

Figure 4 shows representative plan-view images of each of our samples. It is evident that dot-chains exist in all three samples, similar to those reported for uncapped[8,9] and partially-capped QD chains.[10] We analyzed these and other similar plan-view TEM images to obtain average values and standard deviations within the populations for the various parameters describing the dots' morphology. Dot widths were obtained as full-width half-max (FWHM) values via the software program ImageJ. Specifically, intensity line profiles were first plotted, which due to the apparent shadowing caused by the TEM (i.e. different facets interacting with the (220) beam condition differently) had a sigmoidal profile. The sigmoidal curves were then differentiated to obtain a Gaussian-like dot profile, from which the FWHM was extracted and recorded as the dot size. This was done with 30 measurements per sample in a random selection of visible dots over three or four

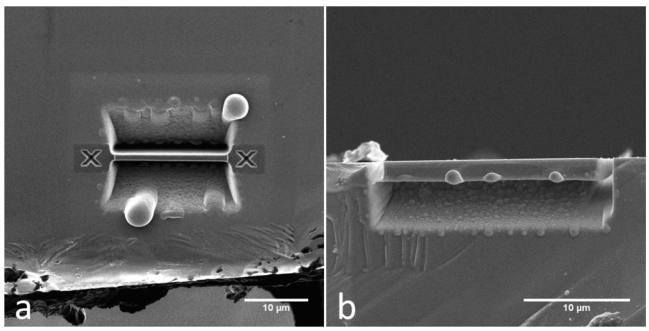

FIG. 2. Lift-out cuts in preparation in the FIB/SEM. (a) A cross-section cut is prepared by milling out pits on both sides of the desired area. This image is a top-down view in the [001] direction. (b) A plan-view cut is prepared by milling out the area underneath the desired cut. This image is looking at a [110] surface of our sample. Since the dots are approximately 100 nm from the top surface the cut was prepared as a wedge, tapering in as it goes away from the [110] surface. The thinnest portion of the cut was then studied in the TEM.

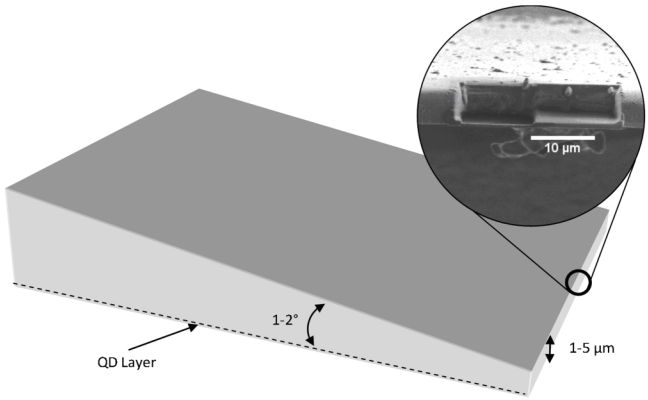

FIG. 3. Diagram of a sample prepared using the hybrid method. Mechanical thinning was done from the underside of the sample (i.e. the top of this diagram) at a small angle from the surface. Once the mechanical thinning limits were reached (1 – 5 μm), the FIB/SEM was used for the final milling and cutting (see inset).

images per sample. The average values and standard deviations are given in Table I. Dot separations within a chain and the number of chains per unit length were similarly measured, and total dot density (dots/cm^2) was calculated by multiplying the inverse of the former by the latter. These values are also given in Table I. To summarize, samples A and B had very similar dot widths (10-11 nm), dot separations (11 nm), chain densities (3×10^5 cm^{-1}), and dot densities ($2 - 3 \times 10^{11}$ cm^{-2}). Conversely, the dots in sample C were substantially larger (25 nm) and more separated (34 nm), had a lower density of chains (2×10^5 cm^{-1}), and a lower overall density of dots (0.6×10^{11} cm^{-2}). As is evident, there is a significant difference in morphology between the two types of dots.

Comparing these samples with others in the literature, we find that the dot density in samples A and B is extremely high. It is smaller than GaAs dots prepared by low temperature droplet epitaxy (7.3×10^{11} cm^{-2}) but larger than any others reported using strain-driven self-assembly (1.4×10^{11} cm^{-2} maximum).[23,24] In addition, images from our samples don't show the large clumps of dots which have been a problem in other low-temperature SK-grown samples when the density becomes larger than 7.5×10^{10} cm^{-2}.[24] The authors of Reference 24 indicated that the presence of clumps was the main reason why their high density dots are not suitable for solar cell applications, namely that the high strain induced by the large clumps penetrates into the upper layers during stacking, generating nonradiative recombination centers and decreasing the radiative conversion efficiency. In contrast, our dots show high optical quality, demonstrated by narrow PL linewidths and light emission from these dots at room temperature.[19]

The observed dot size for samples A and B is comparable to the size of the GaAs dots mentioned above grown via low temperature droplet epitaxy.[23] Those dots were grown on GaAs(311) substrates at temperatures below 100°C, and were extremely closely packed; a dot density of 7.3×10^{11} cm^{-2} yields an average dot separation distance of 11.7 nm. Our dots are as closely packed along the chain direction, 11 ± 2 nm, but overall less closely packed due to the separation between chains. The difference is undoubtedly due to the strain-driven nature of our process, the formation being

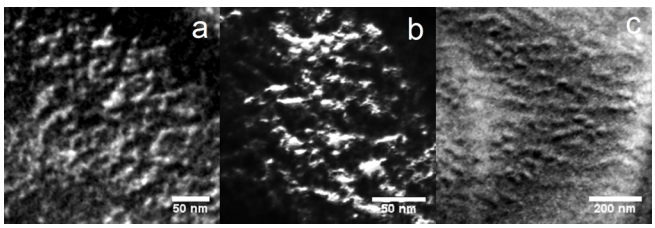

FIG. 4. TEM images of QD chains seen in plan-view cuts from the samples annealed at (a) 460°C, (b) 480°C, and (c) 500°C. Note the difference in scale between (c) compared to (a) and (b).

TABLE I. Physical measurements taken from the plan-view TEM images.

Sample	Dot widths (FWHM, nm)	Dot separation (nm)	Dot-chain density ($\times 10^5$ cm^{-1})	Dot density ($\times 10^{11}$ cm^{-2})
A (460°C)	10.7 ± 2.3	11.0 ± 1.9	2.7 ± 1.4	2.4 ± 1.3
B (480°C)	10.2 ± 1.7	11.1 ± 2.7	3.0 ± 0.8	2.7 ± 1.0
C (500°C)	24.8 ± 4.9	34.4 ± 12.9	1.9 ± 0.2	0.6 ± 0.2

mediated by the mean strain field[25] coupled with elastic relaxation that prefers elongated structures such as quantum wires,[26] as opposed to the non strain-based droplet epitaxy used by that group.

Figure 5 presents a scanning tunneling microscope (STM) image, as-deposited, of a sample similar to samples A, B, and C, taken prior to annealing and dot formation. One monolayer thick platelets are visible. A comparison of this and other STM images from the InGaAs epilayers with the TEM images of the capped QD-chains indicate that the platelet density is the same as the dot density of samples A and B. This suggests that the platelets are precursors of the dots, something which also has been proposed by numerous theoretical works.[25,27–29] The platelets develop into dots during the subsequent capping processes at higher temperatures in samples A and B, while they grow into dots during the ramping up and annealing period in sample C. The apparent discrepancy between the STM images of platelet precursors being randomly distributed and the finished dots appearing in chains may be explained by the dot formation, once allowed to take place, being driven into elongated shapes to better provide elastic relaxation of stress similar to what has been seen in quantum wires.[26]

Figure 6 shows representative cross-section images for our three samples. The light and dark regions indicate the presence of localized strain fields, which again confirm the existence of individual quantum dots in all three samples. The contrasting regions occur as the lattice bends into different Bragg conditions; i.e. the dark region is farther from the (220) condition than the white

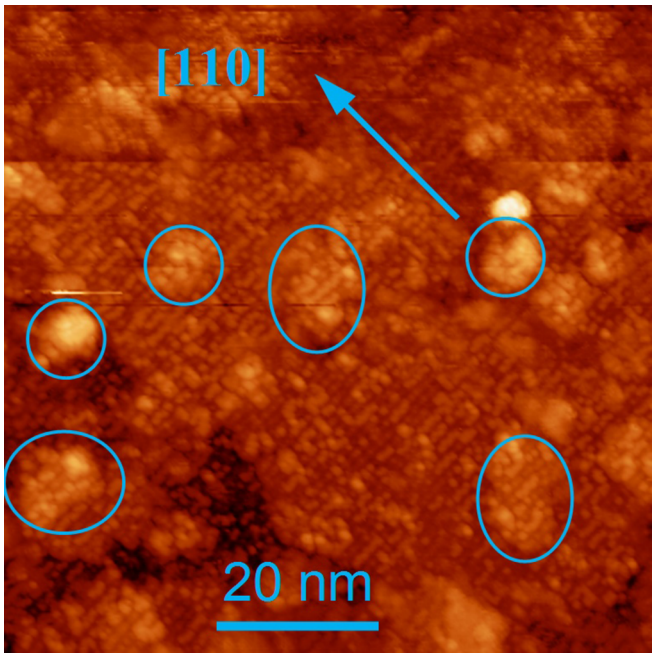

FIG. 5. High resolution, in-vacuum STM image from an as-grown InGaAs surface. The InGaAs epilayer thickness is 10.24 ML, grown on GaAs(001) at low temperature (360°C). The arrow is along the [110] direction. The circles denote the positions of platelets that are 1 monolayer thick.

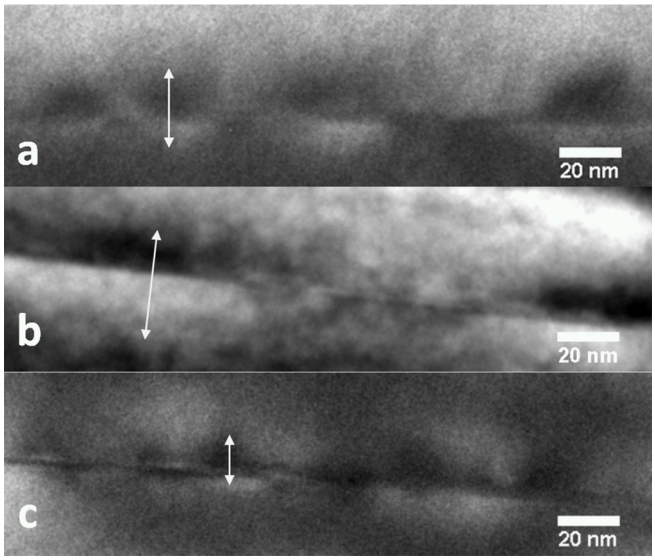

FIG. 6. TEM images of strains of QDs seen in cross-section cuts from the samples annealed at (a) 460°C, (b) 480°C, and (c) 500°C. This image is looking at a $[1\bar{1}0]$ surface of our sample, where the chains and the indium-containing plane extend "into the page". The vertical direction perpendicular to the indium-containing plane is [001]. The white arrows indicate the extent of the strain fields, providing an upper bound on the height of the dots.

region. The white arrows in the images indicate our estimates for the strain fields for some representative cases. Since the strain fields extend beyond the QDs themselves, our measurements of the extent of the strain provide only an upper bound on the height of the dots. Measurements of the strain field heights across many images are 21.7 ± 4.1 nm, 30.8 ± 5.0 nm and 13.8 ± 3.6 nm for samples A, B, and C respectively. These numbers can only roughly be compared, however, since imaging and sample conditions such as sample thickness, sample warping, or being "off-zone" may contribute to how much of the strain fields are visible—so, for example, we cannot conclude that the dots in sample B are taller than the dots in sample A (they may well be shorter, as is discussed in a later paragraph). Roughly speaking, however, this seems to indicate that sample C contains flatter dots than samples A and B.

The cross-section cuts were also used for the EDS measurements on chemical composition to determine the distribution of indium in the samples. As mentioned above, line measurements were done as a series of point measurements across the indium-containing region (wetting layer and dots). Since the EDS beam probes all the way through the cross-section, a large percentage of the volume being probed will be GaAs in addition to InGaAs; therefore, the EDS measurements can be used to verify the presence and measure the distribution of indium, but not to establish the specific indium composition percentage. The EDS results are presented in Figure 7. The curves in the figure have been normalized, shifted vertically for clarity, and fitted to Gaussian curves. A summary of the strain field measurements and the indium distribution widths is found in Table II. (The reported indium distribution widths are the $1/e^2$ widths from the Gaussian fits.)

If the indium were distributed uniformly throughout the dots, one would expect the base of the dots (left hand side of the displayed peaks in Fig. 7) to have a higher amount of indium than the peak of the dots (right hand side), and the peaks in Fig. 7 would be asymmetric. This is because as the TEM passes through the base of the dots, a greater fraction of the material being probed is InGaAs dots and a smaller fraction is GaAs barrier. In our measured data of Fig. 7 there may be a slight asymmetry present, skewed in that direction, but if so it is small—as is evidenced by the ability of the Gaussian curves to adequately fit the data. The presence of symmetry in the Fig. 7 peaks therefore seems to indicate that the indium is segregating vertically, i.e. rising towards the tops of the dots. This is consistent with the concept of "floating indium",[30] and uneven distribution of indium in QDs due to segregation has been reported in other samples—for example, in measurements from energy selective imaging in uncapped InGaAs QDs[12] and cross-sectional scanning tunneling

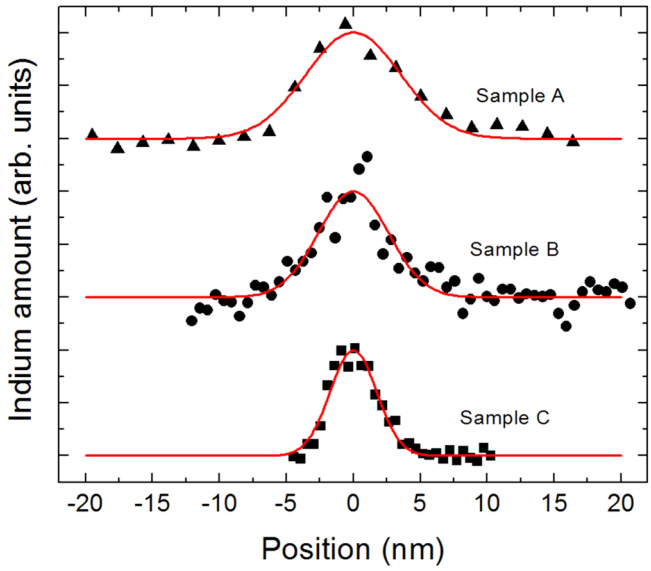

FIG. 7. EDS line scans through the InGaAs sections (wetting layer and dots) of samples A, B, and C (460°C, 480°C, and 500°C), showing amount of indium present. The solid lines are Gaussian fits to the data.

microscopy (STM) of capped InGaAs QDs.[31] However, the low temperature growth should suppress the segregation process. Our findings therefore indicate that the higher temperatures in the later stages (annealing and subsequent capping) are sufficient to allow for indium atoms to rise to the top of the dots.

The measured $1/e^2$ widths of the indium distributions in our samples are 7.1 nm, 5.3 nm, and 3.5 nm, for samples A, B, and C, respectively. All three of these numbers are less than the measured heights of QDs in a similar, uncapped sample annealed at 460°C, measured through STM (8.3 nm, Ref. 8). Therefore it seems likely little or no intermixing of indium with the surrounding GaAs is occurring despite the higher annealing temperatures (for samples B and C; sample A is the same) and even higher temperatures during final capping (for all three samples). Those widths therefore provide a lower bound estimate of the height of the dots, the strictness of the bound being determined by the degree of segregation. These results support the indication from the strain field measurements mentioned above that sample C's dots are flatter than the others, and may well indicate that sample B's dots are flatter than sample A's. This is consistent with our PL peak position data which found that sample C had the highest PL peak energy, followed by sample B and then sample A.[19] Since all three samples have the same nominal indium concentration, the dominant factor in establishing differences in peak position will be quantum confinement, particularly in the smallest dimension. Sample C therefore has the largest quantum confinement shift in PL energy due to the very short height of its dots (despite its overall greater average volume per dot). This assignment of dot heights being shortest for C, then B, then A, also matches the findings of Kim *et al.*, who reported a flattening of dots in other dot-chain samples with increasing annealing temperature.[8]

When the cross-section data is combined with the plan-view data, they then indicate sample C has larger dot width, smaller dot height, larger separation between dots, larger chain separations, and a much smaller overall dot density compared to samples A and B. These differences can all

TABLE II. Physical measurements taken from the cross-section TEM images.

Sample	Strain field height (nm)	Indium region height (nm)
A (460°C)	21.7 ± 4.1	7.1 ± 0.6
B (480°C)	30.8 ± 5.0	5.3 ± 0.4
C (500°C)	13.8 ± 3.6	3.5 ± 0.2

be explained by Ostwald ripening occurring in sample C during the 120 second annealing period. Ostwald ripening, i.e. the growth of larger particles at the expense of smaller seed particles, has been shown to occur in Si/Ge systems (Ge islands on Si substrate) in time scales of 20 seconds.[32] In an InGaAs system, namely InGaAs islands on a GaAs substrate and an annealing temperature of 450°C, substantial ripening occurred in 5 minutes.[33] Our sample C was annealed at a temperature of 500°C, thus one would expect shorter ripening times than their time of 5 minutes. Our observations of larger dots in sample C therefore make sense with substantial ripening having occurred during the 120 second annealing period. Samples A and B, conversely, exhibited no ripening. This verifies the RHEED data from Ref. 19 (mentioned above) which suggested that the dots in samples A and B had not yet formed during the 120 s period of annealing. If the dots form later in the growth, then there is not enough time at high temperatures for ripening to occur.

As we have mentioned above, samples A and B exhibited much better optical properties than sample C, and (similarly) much better than the typical SK grown dots. Moreover, the optical data led us to propose that samples A and B may have a much more uniform size distribution than sample C.[19] These TEM data don't support that hypothesis for the lateral dimensions; the uniformity of the size distribution, as measured by the ratio of the population standard deviation to average dot width, is fairly comparable for all three dots. However, for the out-of-plane dimension (i.e. the heights), sample C did have a noticeably larger non-uniformity in its strain profiles than samples A and B, as measured by a similar ratio. Its standard deviation/height ratio is 26%, compared to 19% and 16% for samples A and B, respectively. Although the out-of-plane measurements are not as precise as the lateral measurements (as discussed above), this is at least consistent with the dots in samples A and B being more uniform in their optical properties. Since quantum confinement effects depend very strongly and nonlinearly on structural dimensions, and since this is the smallest dimension of the QDs, any non-uniformity in this dimension will have magnified effects in the electronic and hence optical uniformity. The data therefore indicate that in order to produce dots with the best possible optical properties, one should emphasize growth techniques which cause less flattening of the dots.

In conclusion, we have used TEM techniques to make quantitative structural and compositional measurements in self-assembled InGaAs QD chains. The TEM results demonstrate that the morphology of the dots annealed at 460°C and 480°C is quite similar, but the morphology changes abruptly as the annealing temperature is raised from 480°C to 500°C. In other words, there is a critical annealing temperature above which the dots flatten out, the widths increase, the heights decrease, and both the dot density within the chains and the dot-chain density decrease. This is consistent with, and explained by, previous results which indicated that the SK transition to dots occurs at a later point in the growth process for the 460°C and 480°C annealed samples compared to the 500°C sample. The 500°C sample features substantial Ostwald ripening due to its earlier dot formation and relatively high annealing temperature. EDS measurements on indium concentration support the claim that this modified SK method creates dots with little intermixing into the surrounding GaAs, but may indicate indium segregation towards the peak of the pyramidal dots is still occurring. The 460°C and 480°C samples additionally have very good optical properties, as reported earlier; thus this structural data indicates that small dots, closely spaced into chains, but without the clumping that can occur in other strain-driven methods, can be a good system for future optical device applications.

ACKNOWLEDGMENT

The work is supported by the National Aeronautics and Space Administration (Cooperative Agreement Number: NNX13AD31A). Also financial support from the National Science Foundation, grant numbers 0854313, 0903804 and 114 3543 is gratefully acknowledged.

[1] M. A. Reed, J. N. Randal, R. J. Aggarwal, R. J. Matyi, T. M. Moore, and A. E. Wetsel, "Obseration of discrete electronic states in a zero-dimensional semiconductor nanostructure," Physical Review Letters **60**, 535 (1988).

[2] V. A. Egorov, G. E. Cirlin, N. K. Polyakov, V. N. Petrov, A. A. Tonkikh, B. V. Volovik, Y. G. Musikhin, A. E. Zhukov, A. F. Tsatsulnikov, and V. M. Ustinov, "1.3 – 1.4 μm photoluminescence emission from InAs/GaAs quantum dot multilayer structures grown on GaAs singular and vicinal substrates," Nanotechnology **11**, 323–326 (2000).

[3] H. C. Liu, M. Gao, J. McCaffrey, Z. R. Wasilewski, and S. Fafard, "Quantum dot infrared photodetectors," Applied Physics Letters **78**, 79–81 (2001).
[4] P. Bhattacharya, S. Ghosh, and A. Stiff-Roberts, "Quantum dot opto-electronic devices," Annu. Rev. Mater. Res. **34**, 1–40 (2004).
[5] S. Bose, "Quantum communication through an unmodulated spin chain," Physical Review Letters **91**, 1–4 (2003).
[6] Y. Li, O. Voskoboynikov, C. P. Lee, S. M. Sze, and O. Tretyak, "Electron energy state dependence on the shape and size of semiconductor quantum dots," Journal of Applied Physics **90**, 12 (2001).
[7] I. N. Stranski and L. von Krastanow, Abhandlungen der Mathematisch-Naturwissenschentlichen Klasse IIb **146**, 797–810 (1938).
[8] D. J. Kim, E. A. Everett, and H. Yang, "Annealing induced transition of flat strained InGaAs epilayers into three-dimensional islands," Journal of Applied Physics **101**, 106106 (2007).
[9] D. J. Kim and H. Yang, "Shape control of InGaAs nanostructures on nominal GaAs(001): dashes and dots," Nanotechnology **19**, 475601 (2008).
[10] K. N. Chauhan, D. M. Riffe, E. A. Everett, D. J. Kim, H. Yang, and F. K. Shen, "Carrier capture dynamics of single InGaAs/GaAs quantum-dot layers," Journal of Applied Physics **113**, 203710 (2013).
[11] O. G. Schmidt, O. Kienzle, Y. Hao, K. Eberl, and F. Ernst, "Modified Stranski-Krastanov growth in stacked layers of self-assembled islands," Applied Physics Letters **74**, 1272–1274 (1999).
[12] T. Walther, A. G. Cullis, D. J. Norris, and M. Hopkinson, "Nature of the Stranski-Krastanow transition during epitaxy of InGaAs on GaAs," Physical Review Letters **86**, 2381–2384 (2001).
[13] G. Biasiol, S. Heun, G. B. Golinelli, A. Locatelli, T. O. Mentes, F. Z. Guo, C. Hofer, C. Teichert, and L. Sorba, "Surface compositional gradients of InAs/GaAs quantum dots," Applied Physical Letters **87**, 223106 (2005).
[14] T. V. Hakkarainen, J. Tommila, A. Schramm, A. Tukiainen, R. Ahorinta, M. Dumitrescu, and M. Guina, "Structural characterization of InAs quantum dot chains grown by molecular beam epitaxy on nanoimprint lithography patterned GaAs(100)," Nanotechnology **22**, 295604 (2001).
[15] E. Uccelli, M. Bichler, S. Nürnberger, G. Abstreiter, and A. F. i Morral, "Controlled synthesis of InAs wires, dot, and twin-dot array configurations by cleaved edge overgrowth," Nanotechnology **19**, 045303 (2008).
[16] P. M. Petroff and S. P. DenBaars, "MBE and MOCVD growth and properties of self-assmebling quantum dot arrays in III-V semiconductor structures," Superlattices and Microstructures **15**, 1 (1994).
[17] Z. M. Wang, K. Holmes, Y. I. Mazur, and G. Salamo, Applied Physics Letters **84**, 1931 (2004).
[18] T. V. Hakkarainen, A. Schramm, A. Tukiainen, R. Ahorinta, L. Toikkanen, and M. Guina, "Lateral ordering of InAs quantum dots on cross-hatch patterned GaInP," Nanoscale Res. Lett. **5**, 1892 (2010).
[19] H. Yang, D. J. Kim, J. Colton, T. Park, D. Meyer, A. M. Jones, S. Thalman, D. Smith, K. Clark, and S. Brown, Growth and temperature dependent photoluminescence of InGaAs quantum dot chains. Applied Surface Science, available online 14 Jan 2014, ISSN 0169-4332, http://dx.doi.org/10.1016/j.apsusc.2013.12.176.
[20] J. P. McCaffrey, M. D. Robertson, S. Fafard, Z. R. Wasilewski, E. M. Griswold, and L. D. Madsen, "Determination of the size, shape, and composition of indium-flushed self-assembled quantum dots by transmission electron microscopy," Journal of Applied Physics **88**, 2272 (2000).
[21] F. A. Stevie, C. B. Vartuli, L. A. Giannuzi, T. L. Shofner, S. R. Brown, B. Rossie, F. Hillion, R. H. Mills, M. Antonell, R. B. Irwin, and B. M. Purcell, "Application of focused ion beam lift-out specimon preparation to TEM, SEM, STEM, AES, and SIMS analysis," Surface and Interface Analysis **31**, 345–351 (2001).
[22] R. Anderson and S. J. Klepeis, "Combined tripod polishing and FIB method for preparing semiconductor plan view specimens," MRS Proceedings **480**, 187 (1997).
[23] M. Jo, T. Mano, Y. Sakuma, and K. Sakoda, "Extremely high-density GaAs quantum dots grown by droplet epitaxy," Applied Physics Letters **100**, 212113 (2012).
[24] D. Zhou, G. Sharma, S. F. Thomassen, T. W. Reenaas, and B. O. Fimland, "Optimization towards high density quantum dots for intermediate band solar cells grown by molecular beam epitaxy," Applied Physics Letters **96**, 061913 (2010).
[25] Y. Chen and J. Washburn, "Structural transition in large-lattice-mismatch heteroepitaxy," Physical Review Letters **77**, 4046 (1996).
[26] J. Tersoff and R. M. Tromp, "Shape transition in growth of strained islands: spontaneous formation of quantum wires," Physical Review Letters **70**, 2782 (1993).
[27] C. Priester and M. Lannoo, "Origin of self-assembled quantum dots in highly mismatched heteroepitaxy," Physical Review Letters **75**, 93 (1995).
[28] H. T. Dobbs, D. D. Vvedensky, A. Zangwill, J. Johansson, N. Carlsson, and W. Seifert, "Mean-field theory of quantum dot formation," Physical Review Letters **79**, 897 (1997).
[29] A. Li, F. Liu, D. Y. Petrovykh, J.-L. Lin, J. Viernow, F. J. Himpsel, and M. G. Lagally, "Creation of quantum platelets via strain-controlled self-organization at steps," Physical Review Letters **85**, 5380 (2000).
[30] P. Howe, E. C. Le Ru, E. Clarke, R. Murray, and T. S. Jones, "Quantification of segregation and strain effects in In As Ga As quantum dot growth," Journal of Applied Physics **98**, 113511 (2005).
[31] N. Liu, J. Tersoff, O. Baklenov, A. L. Holmes, Jr., and C. K. Shih, "Nonuniform composition profile in $In_{0.5}Ga_{0.5}As$ alloy quantum dots," Physical Review Letters **84**, 334–337 (2000).
[32] F. M. Ross, J. Tersoff, M. Reuter, F. K. Legoues, and R. M. Tromp, "In situ transmission electron microscopy observations of the formation of self-assembled Ge islands on Si," Microscopy Research and Technique **42**, 281–294 (1998).
[33] L. Ke, Z. Qing, Z. Xun, G. Xiang, L. Zi-Jiang, W. Ji-Hong, H. Ming-Zhe, and D. Zhao, "Ripening of single-layer InGaAs islands on GaAs (001)," Chin. Phys. B **22**, 026801 (2013).